Supporting Information for Tailoring $Ca_2Mn_2O_5$ Based Perovskites for Improved Oxygen Evolution Reaction

Neha Bothra,[†,‡] Sandhya Rai,[†,‡] and Swapan K. Pati[*,†]

†*Advanced Quantum Theory: Molecules to Materials Group, School of Advanced Materials (SAMat), Theoretical Science Unit, Jawaharlal Nehru Centre for Advanced Scientific Research, Jakkur, Bengaluru, 560064, India.*

‡*Authors contributed equally*

E-mail: *pati@jncasr.ac.in

S1 Methods

First principles calculations were carried out using Quantum Espresso 5.2.0 package.[1,2] Generalized gradient approximation was incorporated via the exchange correlation functional parameterized by Perdew-Burke-Ernzerhoff (PBE).[3,4] The core electrons are treated in the Rappe-Rabe-Kaxiras-Joannopoulos ultrasoft pseudopotential method.[5] Valence electron configuration for each element is $4s^24p^65s^2$ in Sr, $4d^{10}5s^25p^1$ in In, $5d^{10}6s^26p^3$ in Bi, $5s^25p^65d^16s^2$ in La, $5s^25p^65d^14f^16s^2$ in Ce, $5s^25p^65d^14f^76s^2$ in Eu, $3d^44s^2$ in Mn and $2s^22p^4$ in O. Due to strong correlation of d–electrons in Mn, the Hubbard U correction[6] was applied to Mn with a specific value of 4.0 eV, in accordance with some recent calculations on Mn.[7] Spin polarization was applied on Mn with spin structure as ferromagnetic, as is reported about the spin state for experimentally synthesized $Ca_2Mn_2O_5$.[8] The 3×3×1 Monkhorst

Pack[9] reciprocal grid was used to sample out the total energy numerically. In order to accelerate the computation near the Fermi level, a Methfessel-Paxton smearing of 0.01 was used.[10] The Broyden–Fletcher–Goldfarb–Shanno algorithm[11] was used for full relaxation of the atomic positions of both, slab and adsorbed intermediates. Conjugate gradient method was used for the electronic relaxation and simultaneous DOS, PDOS and Bader charge calculations.[12] The wave function kinetic energy cutoff was 30 Ry, for energy accuracy.

To avoid the asymmetric slab induced dipole moments, all the slabs were constructed symmetrically considering the (001) plane A–Mn–O (A=Ca/Dopants) as the terminating layer. The cell was chosen following a series of calculations, to make sure that the boundary effects are excluded. The inter-adsorbate distance was maintained at more than 5 Å to avoid adsorbate-adsorbate interactions. The 2X1X5 unit cell was finally chosen after checking for the adsorption energy of OH on the surface, for different number of layers. Similar size of unit cells have been used in the previous calculations as well yielding reliable results.[13] Surface Mn was identified as the catalytically active site in all the cases and all the adsorbates, *O, *OO, *OH and *OOH were bonded to Mn. In order to calculate the energy of the ions in solvent, computational hydrogen electrode[14] (CHE) developed by Nørskov *et al.* was used as the reference electrode. In accordance with this model, the concerted step of proton and electron transfer can be converted to the half energy of hydrogen molecule. The same concept has been applied to estimate the energy of (e^- – OH^-).

$$H_2O(l) \longrightarrow H^+(aq) + OH^- \tag{1}$$

From the CHE model electrode theory

$$H^+ + e^- \longrightarrow \frac{1}{2}H_2$$

$$\Delta G_{(H_2O)} = (H^+_{aq} + e^-) + (OH^- - e^-)$$

$$\Delta G_{(H_2O)} = \Delta G_{(\frac{1}{2}H_2)} + (OH^- - e^-)$$

$$\Rightarrow \Delta G_{(H_2O)} - \Delta G_{(\frac{1}{2}H_2)} = (OH^- - e^-) \tag{2}$$

Since the PBE functional predicts over–binded triplet O_2–dimer, the O_2 free energy at 298.15 K was estimated as:

$$\Delta G_{O_2} = 2\{\Delta G_{H_2O} - \Delta G_{H_2}\} \tag{3}$$

In a similar way, the free energy of OH^- was estimated as:

$$\Delta \mathrm{G_{OH^-}} = \frac{1}{2}\{\Delta \mathrm{G_{total}} - \Delta \mathrm{G_{O_2}} - 2\Delta \mathrm{G_{H_2O}}\} \tag{4}$$

where $\Delta G_{total} = 4 \times 1.23\, eV$. Thus, all the electrochemical reaction energies were mapped to the value with reference to reversible hydrogen electrode (RHE). The thermodynamic and entropic aspect was included in the 0K electronic energy of the slab+ adsorbate configuration from the previous works of Montoya *et al.*[15] The equation to calculate Gibbs reaction energy is:

$$\Delta \mathrm{G_r} = \Delta \mathrm{E_{0K}} + \Delta \mathrm{ZPE} + \Delta \mathrm{H_{0K \to 298.15K}} - \mathrm{T}\Delta \mathrm{S_{0K \to 298.15K}} \pm \mathrm{neU} \tag{5}$$

in which the ΔE_{0K} is the reaction energy at 0K, ΔZPE is the reaction energy from zero point vibration, $\Delta H_{0K \to 298.15K}$ and $\Delta S_{0K \to 298.15K}$ are the enthalpy and entropy contribution in bringing the system from 0K to 298.15K, $\pm neU$ is the electrochemical potential energy for 'n' electrons (system reduction +, system oxidation -) under the electrode potential U. It should be noted that for our calculations, all the reactions are considered at U=0 and pH=0. The OER is a 4-electron exchange process and the U^o for all the steps is estimated as:

1. $\mathrm{HO^* + OH^- \longrightarrow O^* + H_2O + e^-}$

   $\mathrm{U_1^o = \Delta G(HO^*) - \Delta G(O^*) - \Delta G(H_2O) - (e^- - OH^-) - eU}$

2. $\mathrm{O^* + OH^- \longrightarrow HOO^* + e^-}$

   $\mathrm{U_2^o = \Delta G(O^*) - \Delta G(HOO^*) - (e^- - OH^-) - eU}$

3. $\mathrm{HOO^* + OH^- \longrightarrow OO* + H_2O + e^-}$

   $\mathrm{U_3^o = \Delta G(HOO^*) - \Delta G(OO^*) - \Delta G(H_2O) - (e^- - OH^-) - eU}$

4. $OO^* + OH^- \longrightarrow HO^* + O_2 + e^-$

   $U_4^o = \Delta G(OO^*) - \Delta G(HO^*) - \Delta G(O_2) - (e^- - OH^-) - eU$

For all the calculations on (un)doped $Ca_2Mn_2O_5$, a 5–atomic layer slab with (001) plane A–O–Mn exposed layer was constructed with 12Å vacuum layer. The (001) surface with transition metal ions has been widely used as a catalytically active and stable surface for simple perovskites in DFT calculations.[16,17] We hypothesize this to be the case of $Ca_2Mn_2O_5$. The simulation slabs used for DFT calculations were fully oxidized and the structures were relaxed. This is inline with other calculations considering the fact that the OER process occurs in KOH where these slabs would expected to be oxidized.

The PDOS for all the pristine catalysts is given in Figures S2 to S5. Only the significant O p–band, Mn d–band are shown. In case of 30% Ce doped catalyst, a dominant O p–band is observed near the valence band maximum. The oxygen p–band centre was calculated based on the PDOS of every system, by intergrating oxygen PDOS over the p–band using:

$$\mathrm{p-band\,centre} = \frac{\int \mathrm{E.f(E)dE}}{\int \mathrm{f(E)dE}} \tag{6}$$

where E is the electronic energy and f(E) is the density of states corresponding to that E. To get the charge density on the atoms, we have used Bader analysis, which is based upon partitioning charge density grid into Bader volume by steepest ascent method.[18]

S1.1 Multiple Regression based predictive model

The supervised machine learning can be divided into two parts: regression and classification, where regression predicts continuous value outputs and classification predicts discrete outputs. Multiple linear regression falls in the first category. This simply corresponds to a linear relationship between two or more variables. When the number of descriptors/variables exceeds 1, it falls in the category of multiple linear regression. We used the Scikit–learn library within python to develop the model.[19] The dataset was randomly split into 70% training set

Table S1: Details of the descriptors used

Descriptor	Description
p–band centre	Calculated based on the PDOS as $\mathrm{p-band\,centre} = \frac{\int \mathrm{E.f(E)dE}}{\int \mathrm{f(E)dE}}$.
Mn–O bond covalency	Average Bader charge difference between the surface Mn and O atoms.
t×% doping	$t = \frac{r_A + r_O}{\sqrt{2}(r_B + r_O)}$ where r_A was the radius of the dopant. This factor was multiplied with percentage doping.
Fermi energy	Highest occupied energy level of a material at absolute zero temperature.

and 30% test set. The model was based on the slope that corresponds to the data of the training set and the y–intercept which again is derived from the training set. The model was evaluated based on the R^2 value. The better the model, R^2 approaches 1.

The importance analysis for the variables was also done in order to evaluate how much impact would a descriptor have on the model. This was done by replacing the value of the descriptor with an average value and see the difference in R^2 before and after the substitution.

S2 Simulated systems

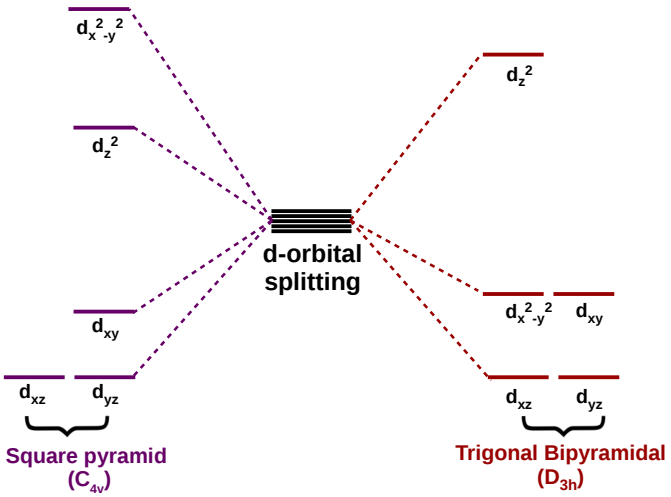

Figure S1: Different crystal-field splitting of d-electrons states for the square pyramid and trigonal bipyramid symmetry around the 5 coordinated Mn ions.

The 5-coordinated geometry can show two different kinds of symmetry, square pyramidal

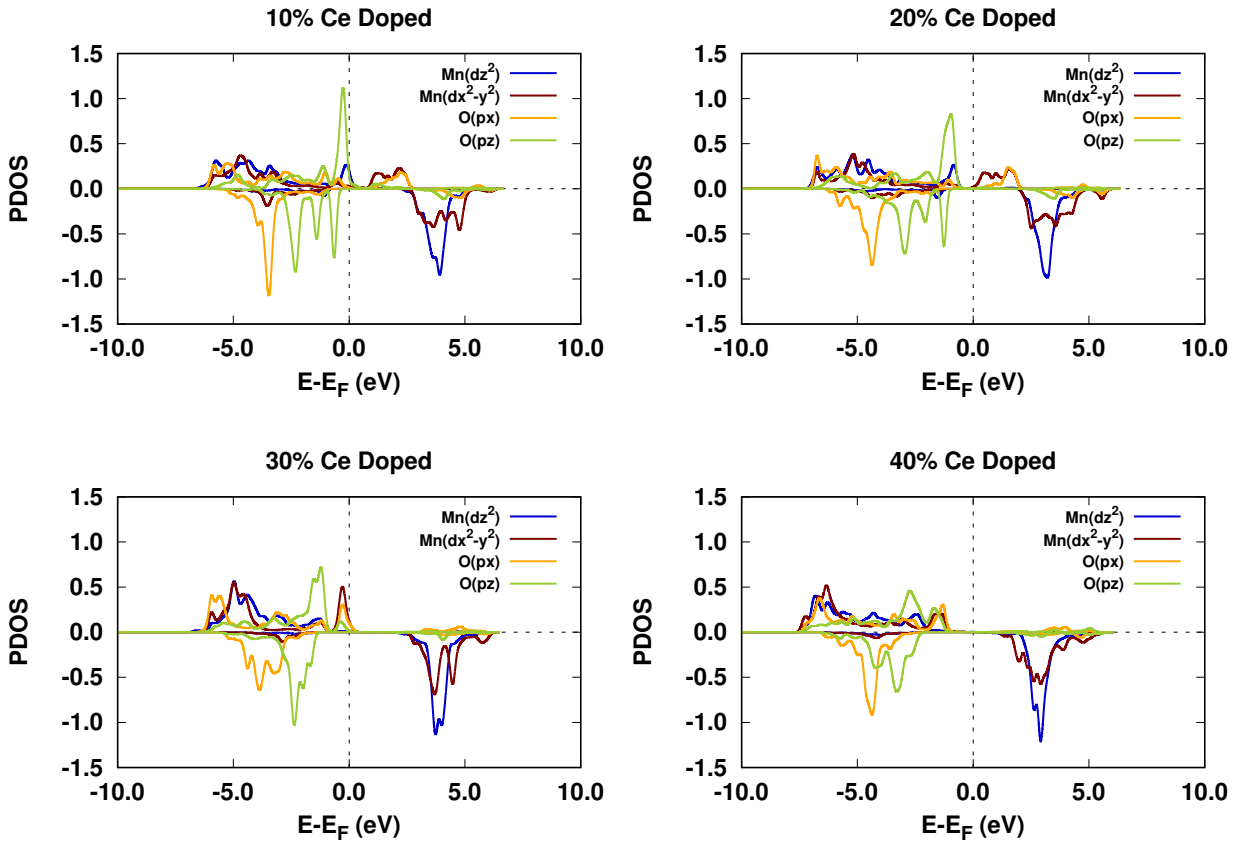

Figure S2: The partial density of states (PDOS) of the Ce doped $Ca_2Mn_2O_5$ of the Mn($d_{x^2-y^2}$), Mn(d_{z^2}) and O(p_z), where Mn is the catalytically active site.

and trigonal bipyramidal. The covalency of the attached ligands decide which of the two geometries will be favoured. This leads to the proper tuning of the orbital alignment and thus controlling the activity of the catalyst. In covalent complexes where presumably the interactions between the bonded pair of electrons are more important than the bonded–non bonded electron pair interactions, the trigonal bipyramidal configuration is favoured. On the other hand, it is essentially the ionic compounds in which the interactions between bonding electron pairs and the d-shell predominates and in which a square pyramidal geometry exists. An important point worth mentioning is that the d^4 configuration is more stable in the bipyramidal geometry rather than the square pyramid.

Table S3 has the data on the p-band centre. As can be seen that the p-band centre is way below the -1.8 eV mark to show instability in OER reaction conditions.[20] The p-band

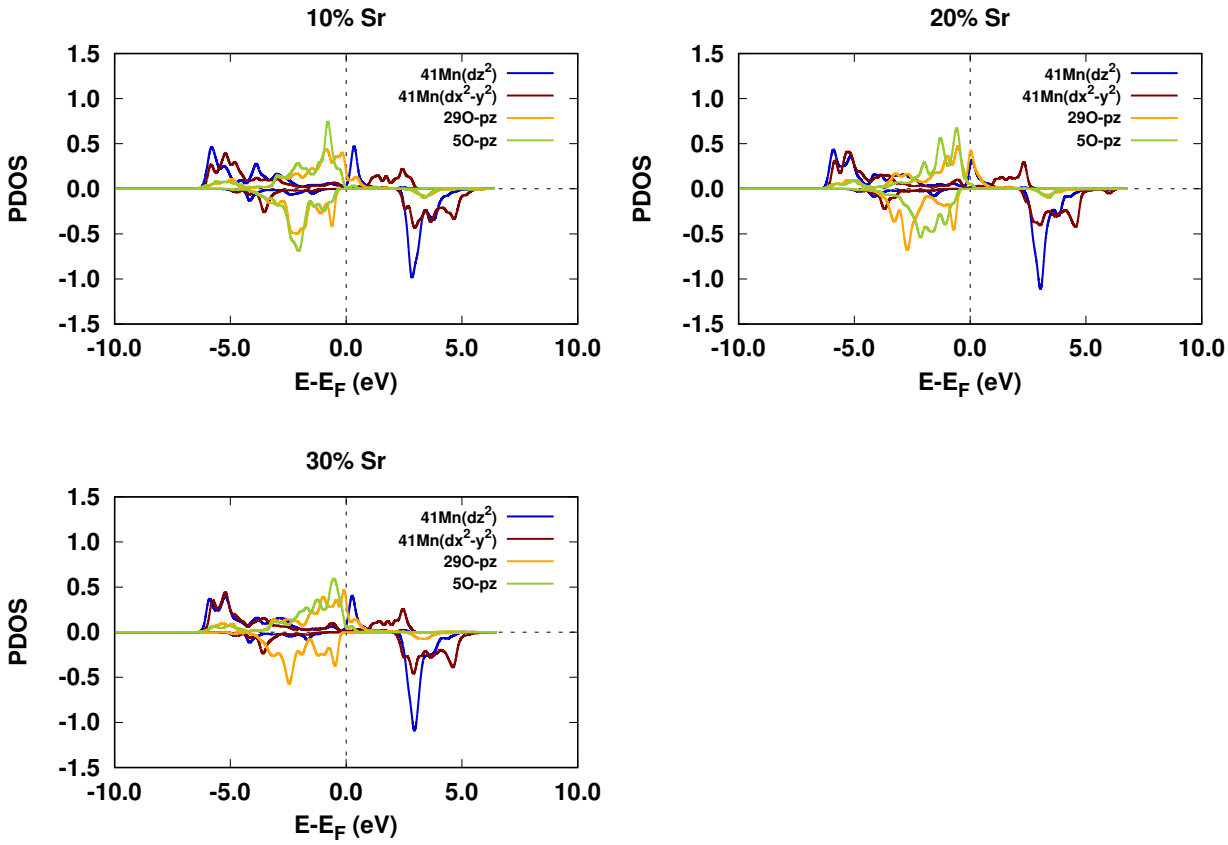

Figure S3: The partial density of states (PDOS) of the Sr doped $Ca_2Mn_2O_5$ of the Mn($d_{x^2-y^2}$), Mn(d_{z^2}) and O(p_z), where Mn is the catalytically active site.

centre and the covalency data also depict the inability of the lattice oxygen to take part in the catalysis.[21,22]

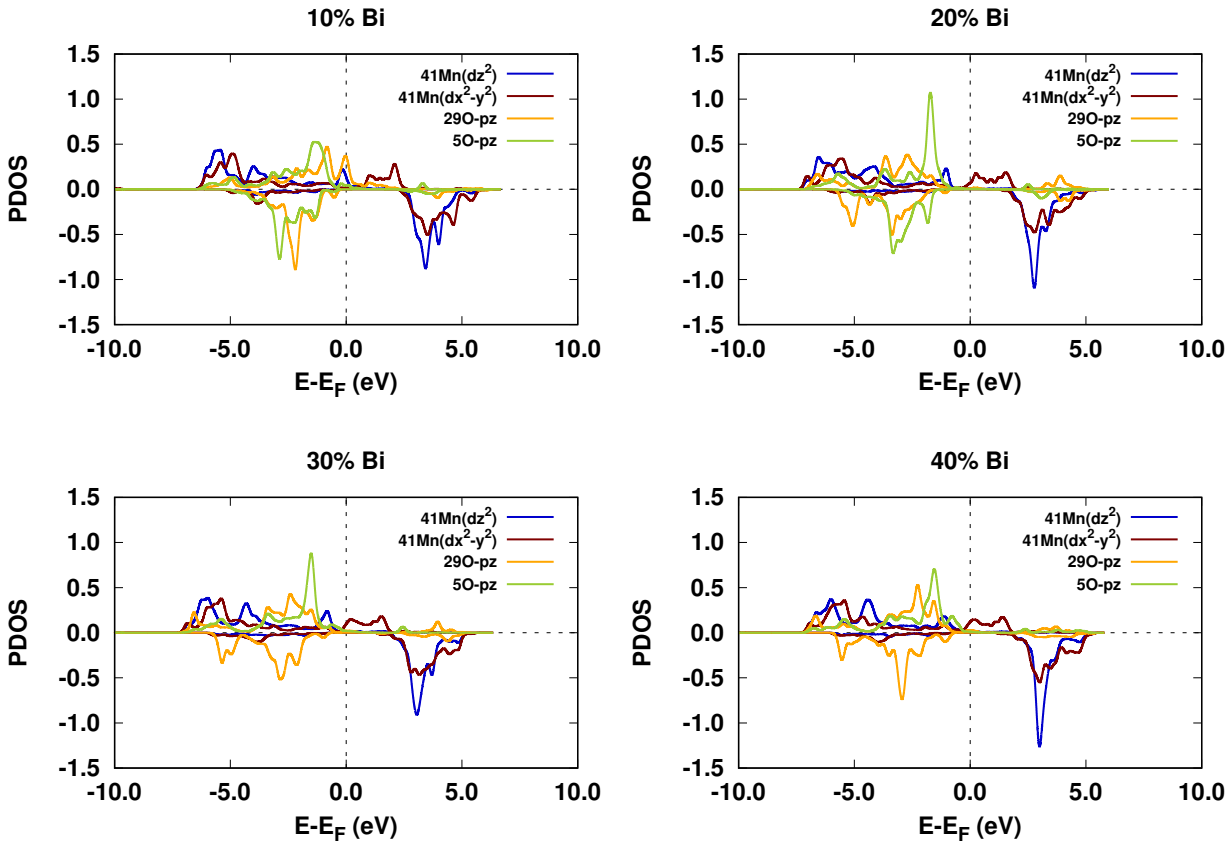

Figure S4: The partial density of states (PDOS) of the Bi doped $Ca_2Mn_2O_5$ of the $Mn(d_{x^2-y^2})$, $Mn(d_{z^2})$ and $O(p_z)$, where Mn is the catalytically active site.

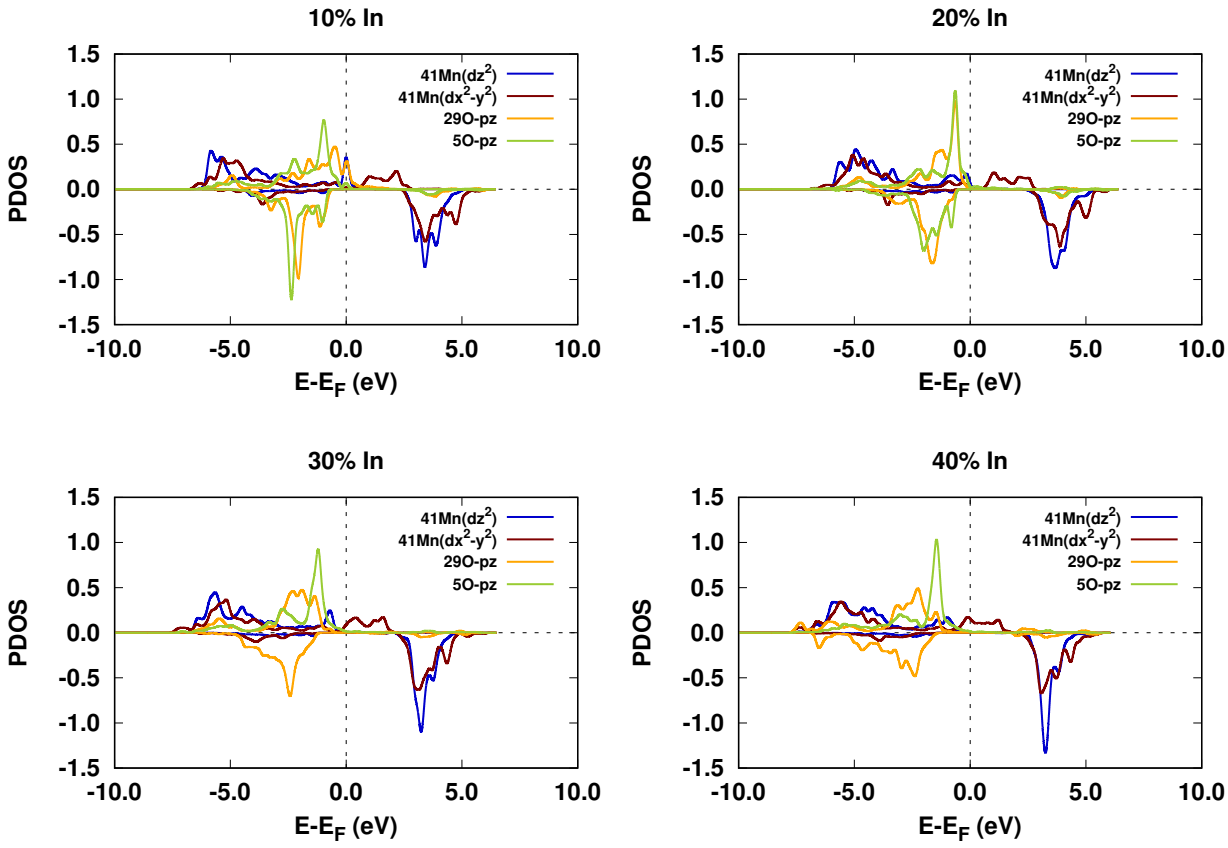

Figure S5: The partial density of states (PDOS) of the In doped $Ca_2Mn_2O_5$ of the $Mn(d_{x^2-y^2})$, $Mn(d_{z^2})$ and $O(p_z)$, where Mn is the catalytically active site.

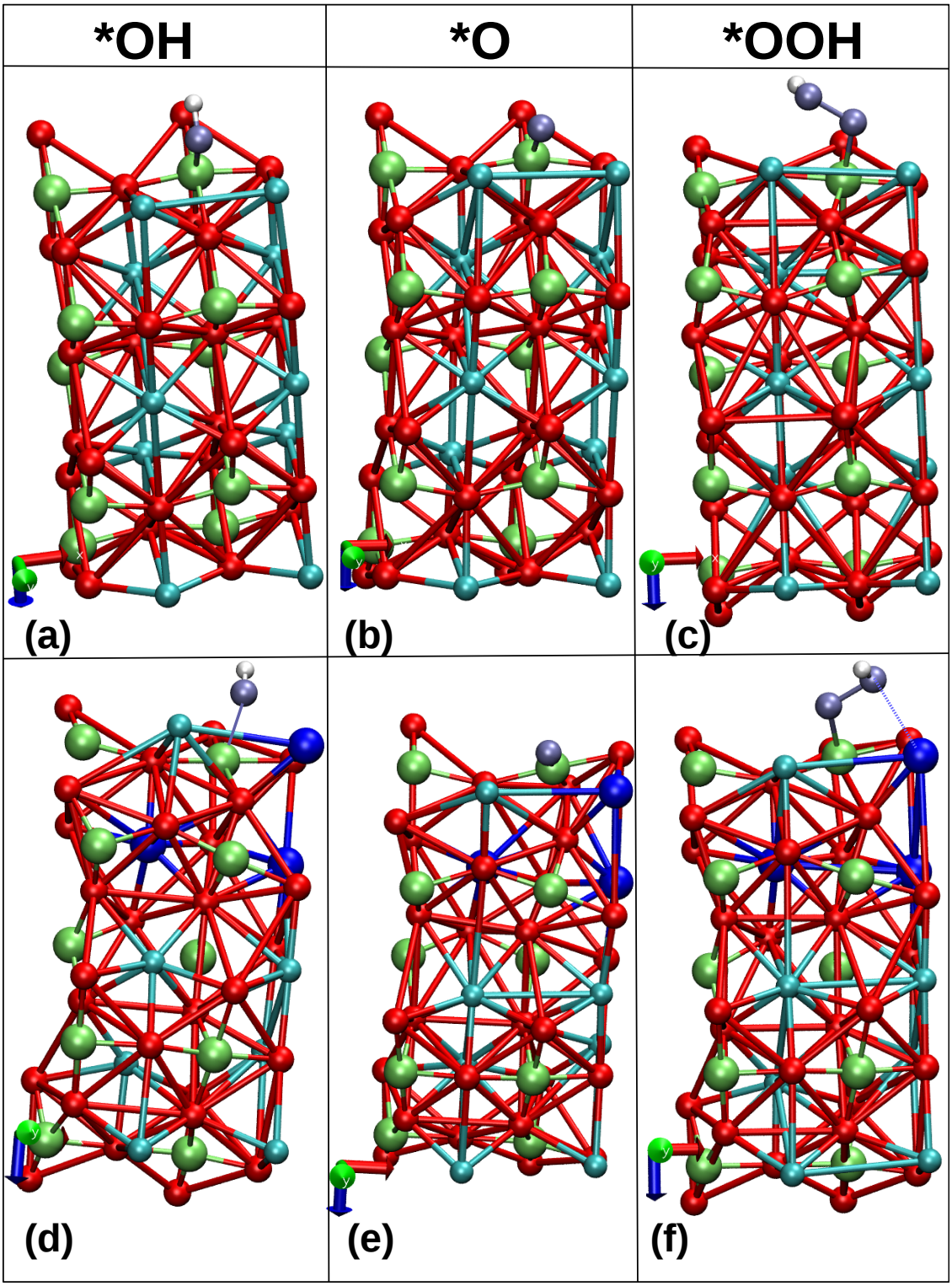

Figure S6: Atomic structures of pristine (a,b,c) and 30% Ce doped (d, e, f) $Ca_2Mn_2O_5$ with adsorbed *OH, *O and *OOH, respectively. The colour code is: deep blue is Ce, limegreen is Mn, Cyan is Ca, Red is O. Adsorbed oxygens are in ice blue colour to differentiate them from lattice oxygen. White ball represents hydrogen. The dotted line shows non–covalent interaction between adsorbed *OOH and lattice oxygen.

Table S2: The standard equilibrium potential (in eV) for the four steps of OER process corresponding to the (un)doped catalysts

System	U_1^o	U_2^o	U_3^o	U_4^o
$Ca_2Mn_2O_5$	1.12	1.49	1.20	1.22
Sr 10%	1.11	1.46	1.19	1.28
In 10%	1.11	1.49	1.21	1.23
Bi 10%	1.12	1.47	1.21	1.24
La 10%	1.11	1.49	1.18	1.24
Ce 10%	1.16	1.46	1.18	1.23
Eu 10%	1.15	1.45	1.24	1.19
Sr 20%	1.11	1.47	1.21	1.24
In 20%	1.11	1.49	1.21	1.22
Bi 20%	1.12	1.47	1.20	1.24
La 20%	1.12	1.47	1.20	1.24
Ce 20%	1.17	1.42	1.23	1.21
Eu 20%	1.13	1.41	1.29	1.21
Sr 30%	1.11	1.47	1.20	1.25
In 30%	1.13	1.46	1.23	1.21
Bi 30%	1.15	1.44	1.21	1.24
La 30%	1.14	1.45	1.19	1.25
Ce 30%	1.21	1.37	1.32	1.13
In 40%	1.12	1.45	1.22	1.24
Bi 40%	1.16	1.43	1.21	1.24
La 40%	1.16	1.43	1.21	1.23
Ce 40%	1.20	1.39	1.22	1.22

Table S3: The data that was used for generating the linear regression based model. The e_g filling was not the part of the final model owing to its inaccuracy in predicting the overpotential (η).

System	η	Fermi level	e_g filling	p-band centre	t×%dope	Covalency
$Ca_2Mn_2O_5$	0.26	2.23	1.03	-2.19	0.00	0.57
10%Sr	0.23	2.48	1.02	-2.23	0.09	0.67
20%Sr	0.24	2.25	1.02	-2.07	0.18	0.62
30%Sr	0.24	2.62	1.02	-2.23	0.27	0.64
10%In	0.26	2.42	1.02	-2.25	0.08	0.57
20%In	0.26	2.46	1.02	-2.17	0.15	0.46
30%In	0.23	2.50	1.03	-2.42	0.23	0.51
40%In	0.22	2.95	1.03	-2.65	0.30	0.43
10%Bi	0.24	2.31	1.02	-2.11	0.08	0.56
20%Bi	0.24	2.60	1.02	-2.22	0.17	0.48
30%Bi	0.21	3.02	1.02	-2.46	0.25	0.53
40%Bi	0.20	3.27	1.02	-2.57	0.34	0.53
10%La	0.26	2.30	1.02	-2.04	0.08	0.60
20%La	0.24	2.48	1.02	-2.11	0.17	0.52
30%La	0.22	3.11	1.03	-2.55	0.25	0.46
40%La	0.20	3.56	1.03	-2.70	0.34	0.40
10%Ce	0.23	2.47	1.03	-2.76	0.08	0.46
20%Ce	0.19	3.11	1.03	-2.62	0.17	0.41
30%Ce	0.14	3.34	1.04	-2.58	0.25	-0.03
40%Ce	0.16	4.24	1.02	-3.02	0.33	-0.06

References

(1) Giannozzi, P.; Baroni, S.; Bonini, N.; Calandra, M.; Car, R.; Cavazzoni, C.; Ceresoli, D.; Chiarotti, G. L.; Cococcioni, M.; Dabo, I. Quantum Espresso: A Modular And Open-Source Software Project For Quantum Simulations Of Materials. *J. Phys.: Condens. Matter* **2009**, *21*, 395502–395508.

(2) Barnes, T. A.; Kurth, T.; Carrier, P.; Wichmann, N.; Prendergast, D.; Kent, P. R.; Deslippe, J. Improved Treatment Of Exact Exchange In Quantum Espresso. *Comput. Phys. Commun.* **2017**, *214*, 52–58.

(3) Ernzerhof, M.; Scuseria, G. E. Assessment of the Perdew–Burke–Ernzerhof Exchange-Correlation Functional. *J. Chem. Phys.* **1999**, *110*, 5029–5036.

(4) Adamo, C.; Barone, V. Toward reliable density functional methods without adjustable parameters: The PBE0 model. *J. Chem. Phys.* **1999**, *110*, 6158–6170.

(5) Rappe, A. M.; Rabe, K. M.; Kaxiras, E.; Joannopoulos, J. Optimized Pseudopotentials. *Phys. Rev. B* **1990**, *41*, 1227–1230.

(6) Dudarev, S.; Botton, G.; Savrasov, S.; Humphreys, C.; Sutton, A. Electron-Energy-Loss Spectra and the Structural Stability of Nickel Oxide: An LSDA+ U Study. *Phys. Rev. B* **1998**, *57*, 1505–1509.

(7) Lee, Y.-L.; Gadre, M. J.; Shao-Horn, Y.; Morgan, D. Ab Initio Gga+ U Study Of Oxygen Evolution And Oxygen Reduction Electrocatalysis On The (001) Surfaces Of Lanthanum Transition Metal Perovskites Labo 3 (B= Cr, Mn, Fe, Co And Ni). *Phys. Chem. Chem. Phys.* **2015**, *17*, 21643–21663.

(8) Kim, J.; Yin, X.; Tsao, K.-C.; Fang, S.; Yang, H. $Ca_2Mn_2O_5$ As Oxygen-Deficient Perovskite Electrocatalyst For Oxygen Evolution Reaction. *J. Am. Chem. Soc.* **2014**, *136*, 14646–14649.

(9) Pack, J. D.; Monkhorst, H. J. Special Points For Brillouin-Zone Integrations - A Reply. *Phys. Rev. B* **1977**, *16*, 1748–1751.

(10) Methfessel, M.; Paxton, A. High-Precision Sampling For Brillouin-Zone Integration In Metals. *Phys. Rev. B* **1989**, *40*, 3616–3621.

(11) Fletcher, R. *Practical Methods Of Optimization*; John Wiley & Sons, 2013.

(12) Arias, T. A.; Payne, M.; Joannopoulos, J. Ab Initio Molecular Dynamics: Analytically Continued Energy Functionals And Insights Into Iterative Solutions. *Phys. Rev. Lett.* **1992**, *69*, 1077–1080.

(13) Zhao, B.; Zhang, L.; Zhen, D.; Yoo, S.; Ding, Y.; Chen, D.; Zhang, Q.; Doyle, B.; Xiong, X.; Liu, M. A Tailored Double Perovskite Nanofiber Catalyst Enables Ultrafast Oxygen Evolution. *Nat. Commun.* **2017**, *8*, 14586.

(14) Nørskov, J. K.; Rossmeisl, J.; Logadottir, A.; Lindqvist, L.; Kitchin, J. R.; Bligaard, T.; Jonsson, H. Origin Of The Overpotential For Oxygen Reduction At A Fuel-Cell Cathode. *J. Phys. Chem B* **2004**, *108*, 17886–17892.

(15) Montoya, J. H.; Garcia-Mota, M.; Nørskov, J. K.; Vojvodic, A. Theoretical Evaluation Of The Surface Electrochemistry Of Perovskites With Promising Photon Absorption Properties For Solar Water Splitting. *Phys. Chem. Chem. Phys.* **2015**, *17*, 2634–2640.

(16) Kushima, A.; Yip, S.; Yildiz, B. Competing Strain Effects In Reactivity Of $LaCoO_3$ With Oxygen. *Phys. Rev. B* **2010**, *82*, 115435–1–115435–6.

(17) Wang, Y.; Cheng, H.-P. Oxygen Reduction Activity On Perovskite Oxide Surfaces: A Comparative First-Principles Study Of LaMnO3, LaFeO3, and LaCrO3. *J. Phys. Chem C* **2013**, *117*, 2106–2112.

(18) Tang, W.; Sanville, E.; Henkelman, G. A Grid-Based Bader Analysis Algorithm without Lattice Bias. *J. Phys.: Condens. Matter* **2009**, *21*, 084204.

(19) Pedregosa, F.; Varoquaux, G.; Gramfort, A.; Michel, V.; Thirion, B.; Grisel, O.; Blondel, M.; Prettenhofer, P.; Weiss, R.; Dubourg, V.; Vanderplas, J.; Passos, A.; Cournapeau, D.; Brucher, M.; Perrot, M.; Duchesnay, E. Scikit-learn: Machine Learning in Python. *J. Mach. Learn. Res.* **2011**, *12*, 2825–2830.

(20) Grimaud, A.; May, K. J.; Carlton, C. E.; Lee, Y.-L.; Risch, M.; Hong, W. T.; Zhou, J.; Shao-Horn, Y. Double Perovskites As A Family Of Highly Active Catalysts For Oxygen Evolution In Alkaline Solution. *Nat. Commun.* **2013**, *4*, 2439–2446.

(21) Grimaud, A.; Diaz-Morales, O.; Han, B.; Hong, W. T.; Lee, Y.-L.; Giordano, L.; Stoerzinger, K. A.; Koper, M. T.; Shao-Horn, Y. Activating Lattice Oxygen Redox Reactions In Metal Oxides To Catalyse Oxygen Evolution. *Nat. Chem.* **2017**, *9*, 457–465.

(22) Yoo, J. S.; Liu, Y.; Rong, X.; Kolpak, A. M. Electronic Origin and Kinetic Feasibility of the Lattice Oxygen Participation During the Oxygen Evolution Reaction on Perovskites. *J. Phys. Chem. Lett.* **2018**, *9*, 1473–1479.